

# LAP: An Attention-Based Module for Faithful Interpretation and Knowledge Injection in Convolutional Neural Networks

Rassa Ghavami Modegh<sup>1,2</sup>, Ahmad Salimi<sup>2</sup>, Alireza Dizaji<sup>2</sup>, Hamid R. Rabiee<sup>\*,1,2</sup>

<sup>1</sup>*DML, Department of Computer Engineering, Sharif University of Technology, Tehran, Iran*

<sup>2</sup>*Department of Computer Engineering, Sharif University of Technology, Tehran, Iran*

## Abstract

Despite the state-of-the-art performance of deep convolutional neural networks, they are susceptible to bias and malfunction in unseen situations. The complex computation behind their reasoning is not sufficiently human-understandable to develop trust. External explainer methods have tried to interpret the network decisions in a human-understandable way, but they are accused of fallacies due to their assumptions and simplifications. On the other side, the inherent self-interpretability of models, while being more robust to the mentioned fallacies, cannot be applied to the already trained models. In this work, we propose a new attention-based pooling layer, called Local Attention Pooling (LAP), that accomplishes self-interpretability and the possibility for knowledge injection without performance loss. Moreover, several weakly-supervised knowledge injection methodologies are provided to enhance the process of training. We verified our claims by evaluating several LAP-extended models on three different datasets, including Imagenet. The proposed framework offers more valid human-understandable and more faithful-to-the-model interpretations than the commonly used white-box explainer methods.

## Index Terms

Self-interpretability, Explainable artificial intelligence, Faithful interpretation, Knowledge Injection, Weak supervision, Convolutional neural networks

## I. INTRODUCTION

As Artificial Intelligence (AI) proved its efficiency and superior-than-humans performance in many fields, its applications have been expanded. Nowadays, AI has entered into real-life applications like clinical computer-aided decision systems, medical diagnosis, and autonomous car driving. These critical applications arose whether AI models are trustable and their decisions are valid. Deep Neural Networks (DNNs), as one of the most successful AI models, make their decisions by complex computations which are not understandable by humans. They are trained end-to-end and are susceptible to learning detours and biases of the dataset rather than the actual concepts and reasons. Since AI has become responsible for making decisions in areas interfering with human rights and ethics, governments have started to make laws about its usages. For example, the European Union has adopted new regulations which enable users to demand an explanation of an algorithmic decision that has affected them [13]. This has strengthened the urge for DNNs to explain themselves. Explaining DNNs have other virtues besides verification of decisions, bias detection, developing trust, and compliance to legislation [5]; it can help in diagnosing the model. Also, knowledge can be discovered from the models with superior-than-human performance to enrich human knowledge [9].

In recent years, there have been many attempts to explain and interpret DNNs' decisions. These studies can be divided into two general areas of intrinsic and post-hoc methods. Intrinsic interpretability is achieved by enforcing interpretability into the model's architecture [31], [40], [43] and the training strategy [8], [10], [17], [43]. In this approach, the model itself can provide explanations for its decisions. These methods do not apply to already trained models [12], [16]. They generally pose limitations over the model's architecture, and some may sacrifice the performance to achieve interpretability [12]. Post-hoc methods try to provide explanations for already trained models. They adopt assumptions and simplifications in their computations that may sacrifice fidelity to achieve more human-understandable explanations [12]. These assumptions also may lead to false interpretations as they may not be valid in the model's decision-making process [35].

Attention-based architectures are a type of intrinsically interpretable architectures. Attention was first used in Natural Language Processing (NLP) to enable a word to take effect from any of the sentence's words without being restricted to their distance [3]. It could provide a score over the words to highlight which words are more important in deciding about another word. Later its applications extended to the field of vision to mimic human attention in tasks such as visual question answering [22] and image captioning [42]. In general, attention provides an importance score over all input tokens. In this work, we utilize the attention mechanism to propose a new pooling layer, easily pluggable into any convolutional neural network (CNN). Our main contributions can be summarized as follows:

- Introducing a new module that is easily pluggable to any CNN, including the already trained networks, that accommodate the model with self-interpretability and the possibility to inject knowledge without restricting the architecture, performance loss, adding parameters to the main-stream of information flow, and increasing order of computations
- Proposing a concept-wise attention mechanism that assigns attention scores to any predefined domain concepts to distinguish the importance of each pixel according to each concept

\*Corresponding author: [rabiee@sharif.edu](mailto:rabiee@sharif.edu)

- Proposing a weakly supervised method for injecting knowledge into the model, useful in shaping the decision-making process of the model leading to more interpretability

## II. RELATED WORKS

### A. Importance based pooling

Pooling layers and strided convolutions are widely used in CNNs to increase the receptive field and decrease memory consumption. Gao et al. have proposed a unified framework for formulating different pooling strategies, called Local Aggregation and Normalization (LAN), and a pooling method called Local Importance Pooling (LIP) [11]. This framework aggregates features within local sliding windows by weighted averaging. The weights are assigned based on the importance of the features. According to this framework, average pooling assumes the same importance score for all the pixels and is susceptible to feature fading. Max pooling assigns one to the highest feature and zeroes to all the others, leading to very sparse gradient paths and slow training. Strided convolutions assign importance based on the pixel's location in the window and are more sensitive to shift variances. LIP has used the attention mechanism to assign importance weights to the features. LIP is applied feature-wise, which makes it different from our proposed architecture. All of the mentioned pooling layers except strided convolutions can lead to loss of relative spatial relations, as they select different features from different spatial locations [27].

### B. Explainability methods

In recent years, many studies have been published about the interpretability and explainability of DNNs. Some of the proposed methods are model-agnostic and treat models as black-boxes. One group of model-agnostic methods mimics the operations of the black-box by training a white-box model and interpreting it instead [38], which is susceptible to errors as the mimicked model does not perform exactly as the primary model. Another group of model-agnostic methods like LIME [29] assesses feature sensitivity by perturbing the feature space around each input which demands an optimization per sample and is computationally inefficient for being applied on many samples with large feature spaces like images.

Model-specific methods work on specific white-box models, meaning they use the architecture and parameters of the model to provide explanations. CAM [45] is only applicable to the networks having one final fully connected layer after the last convolutional layer. It uses the weights of features in the fully connected layer to find the importance of the features for each class and then calculates pixel scores based on their channel-wise activations and the channel importance. Gradient-based methods use gradients of class scores w.r.t the input to find the most sensitive features as if the network is estimated with a Taylor series of order one. The gradients are the weights of the features indicating their importance. Vanilla gradient [34] uses the pure gradients to find important features. It produces a noisy importance map. Guided Backpropagation [36] filters negative gradient flows to bold out the effective pixels. The filtering may lead to false positives. Grad-CAM [32] follows the same steps as CAM, but it uses gradients instead to find the importance of channels which makes it applicable to a broader group of networks. Guided Grad-CAM [32] is a multiplication of Guided Backpropagation and Grad-CAM to produce fine-grained importance maps.

The gradient-based methods suffer from gradient saturation problems leading to near-zero importance scores. Score-based methods like Layer-wise Relevance Propagation (LRP) [4] and Deep Lift [33] propagate scores instead of gradients to calculate the importance of neurons. LRP has defined layer-specific rules to divide the relevance score of the neurons in each layer to their input neurons. The rules assign relevances based on the contribution of the input neurons to the neurons in the next layer. Deep Lift uses a similar procedure to LRP, but it divides the scores based on the difference of the output achieved compared to a baseline input. But it is not easy to define a suitable and meaningful baseline for all applications. Recently, some works have combined the CAM method with score-based interpretations to improve both. Score-CAM [39] adopts a Deep Lift-style scoring scheme to find the channel-wise increase of confidence and then uses the confidence scores in the CAM method. Similar to Score-CAM, Relevance-CAM [20] uses the LRP method to find the importance of channels in any layer and then applies the CAM method to find the corresponding regions in the input. Relevance-CAM has proved its superior performance to other CAM-based methods.

Another group of methods has used attention maps generated by attention mechanisms to explain the model's behavior. This kind of explanation is widely used on Vision Transformers [19] in various domains e.g. pose estimation [41] and medical image diagnosis [24]. A field of research is focused on enhancing transformer explanations by introducing attention flow [2] and relevancy propagation [6], [7] through the layers. There has also been an attempt to make CNN models interpretable by adopting self-attention layers [14], [44]. These attention-based explanation methods are only applicable to either specific architectures they proposed or the Transformers. Therefore they are different from our work which is applicable to any CNN architecture.

## III. METHOD

### A. Local Attention Pool

In general, the attention mechanism conveys the information about the most important parts of the input data. We adopt the attention mechanism in the reduction process of the pooling layers. The process is depicted in Fig. 1a. In contrast to

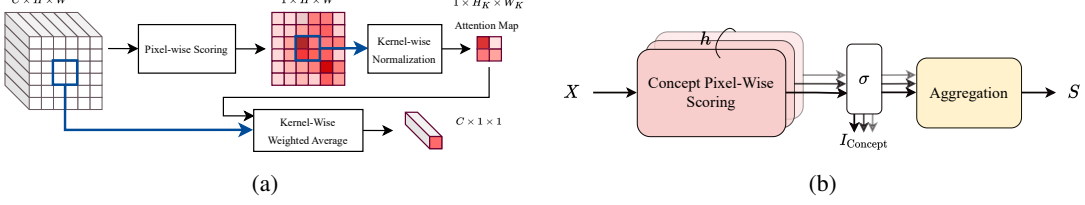


Fig. 1: (a) The local attention pooling is applied on a kernel of size  $W_K \times H_K$  on the input feature map. (b) Multi-concept pixel-wise scoring module aggregates pixel-wise importance maps calculated for all concepts,  $I_{\text{concept}}$ , into a single score map,  $S$ .

LIP, attention is not applied in a channel-wise manner. Instead, the whole feature map is passed to a scoring module to calculate pixel-wise importance scores. Then, the scores related to the pixels under the kernel are normalized for each kernel position. The final feature vector is obtained by weighted averaging the feature vectors of the pixels. This process mimics a zooming action. Instead of mixing the features of the pixels applied to a pooling kernel, the network dynamically detects the most important pixels and passes their features instead. In this way, the small yet important details are not faded or lost but propagated through the network's depth. It also prevents fallacies produced by feature mixing. Different zooming locations under each kernel position may also help in making the model more robust toward shifts and scales.

We have modified the LAN framework to express the pooling procedure of LAP in Eq. (1). In this equation, the output  $O_{i',j'}$  corresponding to a sliding kernel of size  $W_K \times H_K$  with the top-left corner of  $(i, j)$  is calculated based on the input feature map  $X$  related to the pixels under the kernel,  $X_{i:i+H_K,j:j+W_K}$ , and the weighting function  $F$ . In this equation,  $\odot$  stands for element-wise multiplication. The problem with LAN was its calculation of importance weights based on the single values, while LAP uses the whole feature map under a kernel to calculate the weights.

$$\begin{cases} O_{i',j'} = \frac{\sum(F(X_{i:i+H_K,j:j+W_K}) \odot X_{i:i+H_K,j:j+W_K})}{\sum F(X_{i:i+H_K,j:j+W_K})} \\ F : \mathbb{R}^{C \times H_K \times W_K} \rightarrow \mathbb{R}^{H_K \times W_K} \end{cases} \quad (1)$$

In this work,  $F$  combines two steps: the pixel-wise scoring,  $S$ , and local kernel-wise normalization,  $N$ . These steps are presented in Fig. 1a. The general form of  $F$  can be illustrated as Eq. (2) in which  $S$  and  $N$  can be any function.

$$\begin{cases} F(X_{i:i+H_K,j:j+W_K}) = N(V^{i,j}) \\ V^{i,j} = S(X_{i+a,j+b}) \quad \forall 0 \leq a < H_K, 0 \leq b < W_K \\ N : \mathbb{R}^{H_K \times W_K} \rightarrow \mathbb{R}^{H_K \times W_K}; S : \mathbb{R}^C \rightarrow \mathbb{R} \end{cases} \quad (2)$$

Interpretability is one of the well-known benefits of the attention mechanism. Attention scores identify the relative importance of each part of the input. Although any arbitrary scoring function can be used for this purpose, relative importance cannot be interpreted in an absolute way. To achieve the end, we designed a pixel-wise scoring module  $S$  as presented in Fig. 1b. In general, deep models should learn one or more problem-specific concepts to do their tasks, and this architecture helps make the concepts distinguishable by LAPs in the network. In this design, we have considered  $h$  concept scoring heads, each responsible for assigning an importance score to the pixels for their corresponding concept. The sigmoid function is applied over the scores providing concept-wise importance probabilities,  $I_{\text{Concept}}$ . The importance probabilities are then aggregated to calculate the final score. Therefore,  $S$  can be illustrated as Eq. (3), in which  $\sigma$  is the sigmoid function,  $S_C$  is the concept pixel-wise scoring function, and  $A$  is the aggregation function. These concepts may vary based on the domain. Therefore they can be defined by experts. The functions  $S_C$  and  $A$  are also defined based on the concepts;  $S_C$  is a trainable module, but  $A$  can be either trainable or fixed aggregation function like maximum.

$$\begin{cases} S(x) = A(\sigma(S_C(x))) \\ S_C : \mathbb{R}^C \rightarrow \mathbb{R}^h, A : \mathbb{R}^h \rightarrow \mathbb{R} \end{cases} \quad (3)$$

One can adopt any arbitrary method, such as softmax, to normalize the importance scores locally based on the scores of the pixels under the kernel at each position. We have adopted the normalization function:

$$N(V) = e^{-\alpha^2(\max\{V\} - V)^2} \odot V + \epsilon. \quad (4)$$

In this function, the importance probabilities are multiplied by a factor derived from the Gaussian kernel around the highest local importance probability. So the sensitivity toward the most highlighted local pixel becomes adjustable by the trainable parameter  $\alpha$ . Theoretically, when  $\alpha = 0$ ,  $N(V) = V + \epsilon$ , and as  $\alpha \rightarrow \infty$ , the coefficient of the pixels other than  $\max\{V\}$

would approach 0, and LAP would convey the features of the most highlighted local pixel directly. We have added a small value  $\epsilon$  to prevent the weights from becoming zero. This value helps preserve the gradient flow to all pixels and prevents zero division in the weighted averaging process.

CNNs are generally a stack of layers, most of which work by sliding a kernel all over the input and calculating a function. Although the shallower layers have lower receptive fields, they extract fine common details like edges and corners. As the depth increases, the receptive field increases, and the layers become responsible for extracting higher-level concepts [25]. The final decision is made based on the information flow through the layers, and somewhere in the middle, it should have understood the distinguishing concepts. LAP helps specify those concepts besides keeping them bold in the pooling processes. As the importance is identified based on the internal forward flow of the network, LAP modules make the model self-interpretable. LAPs do not produce false positives or negatives due to ignored flows to reach a human-understandable interpretation in contrast to external explainer methods. They also find the important parts in the same direction that the model decides in the forward process.

### B. Knowledge injection

Human experts make their decisions based on special features of the input. For example, jaggedness is one of the factors considered in classifying a tumor as benign or malignant. The neural networks trained freely may or may not have considered all of the reasons in their decision-making. They may have become biased to a dominant feature in the training dataset and loose generalization. LAP provides an easy way for injecting experts' knowledge into the network due to the probabilistic behavior of its scoring module. Experts can highlight the input parts that are important for their decision-making for each concept. The highlighted map can be resized to each LAP's input and used as ground truth to train each concept scoring head. Knowledge injection gives a better guarantee that the network decides based on the factors of the domain.

In most situations, we do not have detailed experts' supervision, but we have a general knowledge about the problem. So the LAP modules can be trained in a weakly supervised manner to behave as desired. Therefore it will also benefit from the gradient injection and fast training. Here, we have used a linear combination of the semi-supervised losses and the main task's loss to train the models, as described below.

1) *Concept-discrimination loss*: For adopting the mentioned loss, we used the design presented in Fig. 1b for the scoring module, with  $h$  concept heads. We assume each sample  $s$  has a set of concepts  $C_s$ . Each concept head highlights the important pixels for the concept, called concept-related clues. To train the concept heads, we considered the following loss terms:

**Min Active Ratio (MinAR).** Each concept head should assign high importance probability to at least a specified portion of the pixels in the samples containing the concept. This makes the model highlight the concept-related clues for the sample.

**Max Active Ratio (MaxAR).** Each concept head should assign high importance probability to at most a specified portion of the pixels in the samples containing the concept, as the main clue is not understandable otherwise. This phenomenon may happen in layers with large receptive fields. As the concept-related clue appears in the receptive fields of all of the pixels, the network may consider all of them as concept-related clues.

**Inactive Ratio (IAR).** Each concept head should assign low importance probability to all the pixels of the samples not containing the concept, as the concept-related clue should not exist in them. This loss can be applied to all the pixels. But because generally, most of the pixels are already inactive in the attention map, this loss term is likely to fade. Therefore, it is better to apply this term on top-scored pixels according to IAR.

Consider a LAP module  $l$  with an input size  $H \times W$ . The loss function for this LAP is shown in Eq. (5). In this equation,  $N_c$  and  $N_{\hat{c}}$  are the number of samples containing and not containing concept  $c$ , respectively.  $k_1 = \lceil \text{MinAR} \times HW \rceil$  and  $k_2 = \lceil (1 - \text{MaxAR}) HW \rceil$  are the numbers of pixels encouraged to have respectively high and low probabilities in the samples containing concept  $c$ , and  $k_3 = \lceil \text{IAR} \times HW \rceil$  is the number of top pixel encouraged to be inactive in other samples.  $\text{top}_{s,k_1}^{l,c}$  and  $\text{bot}_{s,k_2}^{l,c}$  are the sets of pixels of the  $k_1$  high-ranked and  $k_2$  low-ranked pixels of sample  $s$  based on the importance probability of concept head  $c$ .  $p_{s,i,j}^{l,c}$  is the probability of concept head  $c$  for the pixel  $(i, j)$  of sample  $s$ . MinAR, MaxAR, and IAR are hyper-parameters. The first term is multiplied by 2 to balance the effect of positive and negative losses to the concept head  $c$ .

$$- \sum_{c=1}^h \left[ \sum_{s; c \in C_s} \left[ \frac{2 \sum_{(i,j) \in \text{top}_{s,k_1}^{l,c}} \ln(p_{s,i,j}^{l,c})}{k_1 \times N_c} + \frac{\sum_{(i,j) \in \text{bot}_{s,k_2}^{l,c}} \ln(1 - p_{s,i,j}^{l,c})}{k_2 \times N_c} \right] + \sum_{s; c \notin C_s} \frac{\sum_{(i,j) \in \text{top}_{s,k_3}^{l,c}} \ln(1 - p_{s,i,j}^{l,c})}{k_3 \times N_{\hat{c}}} \right] \quad (5)$$

We observed in our experiments that choosing  $\text{top}_{s,k}^{l,c}$  and  $\text{bot}_{s,k}^{l,c}$  sets based on the probabilities assigned by concept head, is sensitive to the initial model parameters. If high weight is considered for concept-discrimination loss, it is likely to get stuck in considering a wrong zone in layers with high receptive fields. To prevent this, we used another module with the same architecture as the scoring module to choose  $\text{top}_{s,k}^{l,c}$  and  $\text{bot}_{s,k}^{l,c}$  sets from. The module, called discriminative scoring module, is trained using the first and third terms of the loss function presented in Eq. (5), without multiplying the first term by 2, and with  $k_1 = k_3 = HW$ . We detached the input of this module to prevent misleading loss injection to the model, as many input parts may be common between the concepts.

2) *Knowledge sharing by concordance loss*: Intuitively, if one LAP layer has found a part of the input as the distinguishing clue for one concept, the proceeding LAP layers should also distinguish the same clue. This fact does not always hold for the previous layers, as they might not have enough understanding to perceive the clue, mainly due to the low receptive field. A human expert can decide whether the receptive field is enough for the LAP layers. In that case, we have used the Jensen-Shannon divergence loss for encouraging the consecutive LAP layers to produce similar maps:

$$\mathcal{JS}(l, s, c) = \frac{1}{2M_s} \sum_{(i,j); |p_{s,i,j}^{l,c} - p_{s,i,j}^{l+1,c}| > t} \left[ (p_{s,i,j}^{l,c} - p_{s,i,j}^{l+1,c}) \ln \frac{p_{s,i,j}^{l,c}}{p_{s,i,j}^{l+1,c}} + (p_{s,i,j}^{l+1,c} - p_{s,i,j}^{l,c}) \ln \frac{1 - p_{s,i,j}^{l,c}}{1 - p_{s,i,j}^{l+1,c}} \right], \quad (6)$$

where  $\mathcal{JS}(l, s, c)$  is the loss for the concept head  $c$  of sample  $s$  between the LAPs  $l$  and  $l + 1$ . The loss is calculated only on the pixels whose importance probabilities in two consecutive LAP layers are more than a specified threshold  $t$ .  $M_s$  is the number of such pixels in sample  $s$ .

Using the Jensen-Shannon loss causes the LAP layers to help each other in finding more clues and the found clues are also more robust. If the receptive field does not suffice in some layer, e.g.,  $l$ , only the pixels with high importance probabilities of  $l$  and low importance probabilities of  $l + 1$  can be used in the Jensen-Shannon divergence loss. We have applied this loss between each pair of consecutive LAP layers.

### C. LAP-Extended Models

LAP is easily pluggable into any convolutional architecture. Pooling and adaptive pooling layers can be replaced directly with LAPs. Strided convolutions can also be replaced by a convolution with the stride of one, proceeding with a LAP with the same kernel size and stride as the convolution's stride. The unique advantage of LAP is that it can be plugged into an already trained model and tuned while other model layers are frozen.

## IV. RESULTS

In the experiments, we aimed to show the general applicability of LAP to different domains and architectures without performance loss and compare its interpretations with state-of-the-art methods for interpreting a model with no or slight modification. To this end, we used three datasets from three different domains. To show the general applicability, we adopted two widely used CNN architectures in our experiments, ResNet [15], and Inception-V3 [37]. While both architectures have high performance, they have different core ideas. ResNet is famous for its residual connections that prepare uninterrupted gradient paths to prevent gradient fading. Inception-V3 is known for its multi-resolution analysis by applying kernels of different sizes to the feature map at each network level. We compared our interpretations with five white-box explainer methods, Guided Back-propagation (GBP), Grad-CAM (GC), Guided Grad-CAM (GGC), Deep Lift (DL), and Relevance-CAM (RC), using implementations of captum [18] in PyTorch [26]. The experiment setup and results for the datasets are presented in the proceeding subsections.

### A. RSNA and CelebA

To explore the general applicability of our method, we investigated its effectiveness in two different domains using RSNA pneumonia detection dataset [1] and Large-scale CelebFaces Attributes (CelebA) dataset [21].

RSNA was published in a Kaggle challenge in 2018. The dataset contains chest X-Ray images of 8851 healthy people, 9555 patients having lung pneumonia, and 11821 patients with other lung abnormalities. The zones related to pneumonia have been specified by experts using bounding boxes. We used the samples related to healthy people and lung pneumonia patients in a classification task. We randomly selected 81% of the data for train, 9% for validation, and 10% for test set.

CelebA dataset is a face attributes detection dataset containing 40 face attributes of celebrity images. We applied binary classification on the smile attribute of this dataset. The dataset consists of 202,599 samples. We randomly selected 70% of the data for train, 10% for validation, and 20% for test set.

ResNet 18 and Inception V3 were used as the base architectures in these tasks. We placed three LAP modules in blocks 2, 3, and 4 of ResNet 18 and maxpool2, Mixed6a, and Mixed7a of Inception V3. The adaptive pooling was replaced with adaptive LAP in both networks. For RSNA, we used two  $1 \times 1$  convolution layers with eight hidden channels and one concept head for detecting pneumonia obligated to be partly active in positive samples and completely inactive in negative ones. As there is only one concept head, there is no need for an aggregation module, and final attention scores are equal to the concept scores. We trained LAP-extended models with two different methods, weak knowledge injection (WS) and experts' knowledge injection (BB). For CelebA, we used three heads to generate concept-wise scores. The first two concept heads refer to negative and positive classes, each obligated to be partially active in its respective class samples and completely inactive otherwise. The third head was added to highlight the common effective pixels with a low concept-discriminability due to the lack of receptive field. The sum of the three heads' scores was used as the aggregation module to generate final attention scores. This dataset

TABLE I: Results on the RSNA, CelebA, and ImageNet datasets for models trained by the proposed weakly supervised loss (WS) and expert annotations (BB). LAP extension has not resulted in performance drop compared to the vanilla models. Accuracies of LAP predictors w.r.t. ground truth (predictivity) and model’s prediction (faithfulness) show their effectiveness.

Dataset	Model	Model performance				LAP predictions				Faithfulness to model			
		Acc.	Sens.	Spec.	BA	LAP <sub>1</sub>	LAP <sub>2</sub>	LAP <sub>3</sub>	LAP <sub>4</sub>	LAP <sub>1</sub>	LAP <sub>2</sub>	LAP <sub>3</sub>	LAP <sub>4</sub>
RSNA	ResNet 18	95.22	95.08	95.37	95.23	-	-	-	-	-	-	-	-
	WS-LAP ResNet 18	96.58	97.07	96.05	96.56	55.48	69.76	88.11	94.41	55.86	70.14	88.6	96.09
	BB-LAP ResNet 18	96.96	95.92	98.08	<b>97</b>	54.06	86.02	95.62	96.8	53.96	85.96	96.42	98.95
	Inception V3	96.15	95.71	96.61	96.16	-	-	-	-	-	-	-	-
	WS-LAP Inception V3	96.63	96.03	97.29	<b>96.66</b>	51.9	51.9	96.15	96.25	51.14	51.14	97.56	97.67
	BB-LAP Inception V3	96.42	96.23	96.61	96.42	51.9	93.65	96.53	96.36	51.57	94.3	99.35	99.73
CelebA	ResNet 18	92.82	90.8	94.7	92.75	-	-	-	-	-	-	-	-
	WS-LAP ResNet 18	92.86	91.6	94.04	<b>92.82</b>	52.32	71.9	88.73	92.57	53.31	73.04	91.34	97.78
	Inception V3	92.8	91.7	93.83	92.77	-	-	-	-	-	-	-	-
	WS-LAP Inception V3	92.98	91.38	94.47	<b>92.92</b>	58.2	92.14	92.92	92.9	57.58	95.91	99.39	99.22
ImageNet	ResNet 50	Top-1 Acc.	Top-5 Acc.	Top-1 Acc.	Top-5 Acc.	Top-1 Acc.	Top-5 Acc.	Top-1 Acc.	Top-5 Acc.	Top-1 Acc.	Top-5 Acc.	Top-1 Acc.	Top-5 Acc.
	LAP ResNet 50 (NFT)	76.13	92.86	-	-	-	-	-	-	-	-	-	-
	LAP ResNet 50 (FT)	75.87	92.74	<b>76.16</b>	92.85	71.98	86.4	-	-	71.98	-	90.83	-

does not provide the bounding-boxes for the images. So, we only trained the LAP-extended models with WS settings. The details of the loss function, training configurations, and hyper-parameters are described in the supplementary.

We evaluated the models using four metrics, accuracy, sensitivity, specificity, and balanced accuracy (BA). Sensitivity and specificity are recall factors for positive and negative classes, respectively. BA is the average of the recalls, which gives a fair metric for imbalanced datasets. The evaluation metrics on test data are presented in Tab. I. In both architectures, the LAP-extended versions have surpassed the performance of the vanilla models.

Each LAP layer can also be used as a standalone predictor. For RSNA, if a LAP has assigned a probability of more than 0.5 to at least one pixel, it means it has found infection in the sample. The prediction of the LAP for these samples is assumed positive and otherwise negative. For CelebA, we took the class with the higher sum of importance scores as the final prediction of the LAP module. We evaluated the predictivity of LAP modules as standalone deciders and the accuracy of their faithfulness to the model’s decisions. According to Tab. I, as expected, the deeper the layer and the larger its receptive field, the higher the predictivity and the faithfulness. In the case of LAP predictivity, the BB-LAPs in both ResNet 18 and Inception V3 generally have higher accuracies than WS-LAPs, especially in LAP<sub>2</sub>. This observation implies that using exact supervision leads to better predictivity in most LAP layers.

To verify the superior performance of our self-interpretation method, we compared the interpretations of the RSNA dataset with five famous white-box explainers, GC, GGC, GBP, DL, and RC. We used experts’ bounding boxes as ground truth to evaluate the interpretations of the methods as a localization task. One of the strong points about our method is its global interpretability, meaning the importance scores have the same scale in all samples, and any score greater than 0.5 is interpreted as important. The other interpretation methods provide relative importance scores and do not provide a cross-sample threshold to distinguish the important pixels from unimportant ones. To find a global threshold for other methods, we normalized each importance map by its maximum value. Then we trained a binary linear classifier based on normalized scores to discriminate the pixels under bounding boxes from the others in the validation set (More details are available in the supplementary). We used the classifier’s threshold to binarize the normalized score maps of the test data. We used intersection over union (IoU) between the binarized interpretation maps and the ground truth bounding boxes to compare the interpretation methods (**Binarization by Thresholding**). As observed in Tab. II, our method has a significantly higher performance than the other methods in both WS-LAP and BB-LAP models, except in BB-LAP Inception V3, in which LAP is slightly outperformed by RC. We also adopted another technique for binarizing the infection maps (**Binarization by Top-Scored Selection**). As ground truth bounding boxes are available, we selected as many top-scored pixels as the bounding boxes area of each sample. Again, LAP has achieved significantly higher performance than the other methods in all models, except in BB-LAP Inception V3, in which LAP is slightly outperformed by RC. We visualized the interpretations of different methods over four examples for BB-LAP Inception V3 in Fig. 2. As this figure presents, LAP interpretations are faithful to the model’s prediction, while GBP and DL have failed to do so. In the true-positive decisions of the model, LAP interpretations have an acceptable overlap with infection bounding boxes, while GC, GGC, and RC have not been successful in capturing all boxes. Details of integrating LAPs (LAP All) and examples of the other models are provided in the supplementary.

### B. Imagenet

In this experiment, we explored the adaptability of our LAPs in already trained models. We chose the ImageNet classification task [30] to assess whether the LAPs can handle interpretations of objects with high variance in size. We used pre-trained ResNet 50 from the torchvision model zoo [23] as the base architecture. Generally, the objects of the ImageNet dataset may have a larger size than the receptive field of the first three layers. Therefore, we only used a LAP in the fourth layer. We used

TABLE II: IoUs of infection bounding boxes of RSNA and binarized interpretation maps of different interpretation methods using two binarization approaches for four networks. LAP achieved a superior performance than other interpretation methods.

Binarization Method	Thresholding						Top-Scored Selection					
	Model	DL	GGC	GC	GBP	RC	LAP	DL	GGC	GC	GBP	RC
WS-LAP ResNet 18	24.37	15.98	9.34	19.09	28.49	<b>36.26</b>	20.44	15.53	7.14	15.55	33.02	<b>44.29</b>
BB-LAP ResNet 18	26.18	16.92	2.2	18.67	17.75	<b>46.5</b>	22.54	16.05	10.27	15.3	20.21	<b>58.61</b>
WS-LAP Inception V3	25.56	22.07	2.04	25.71	<b>33.35</b>	31.97	22.94	20.83	7.82	20.42	<b>41.52</b>	40.72
BB-LAP Inception V3	28.75	15.97	8.44	16.85	34.4	<b>46.94</b>	24.27	12.85	15.59	11.92	41.43	<b>59.86</b>

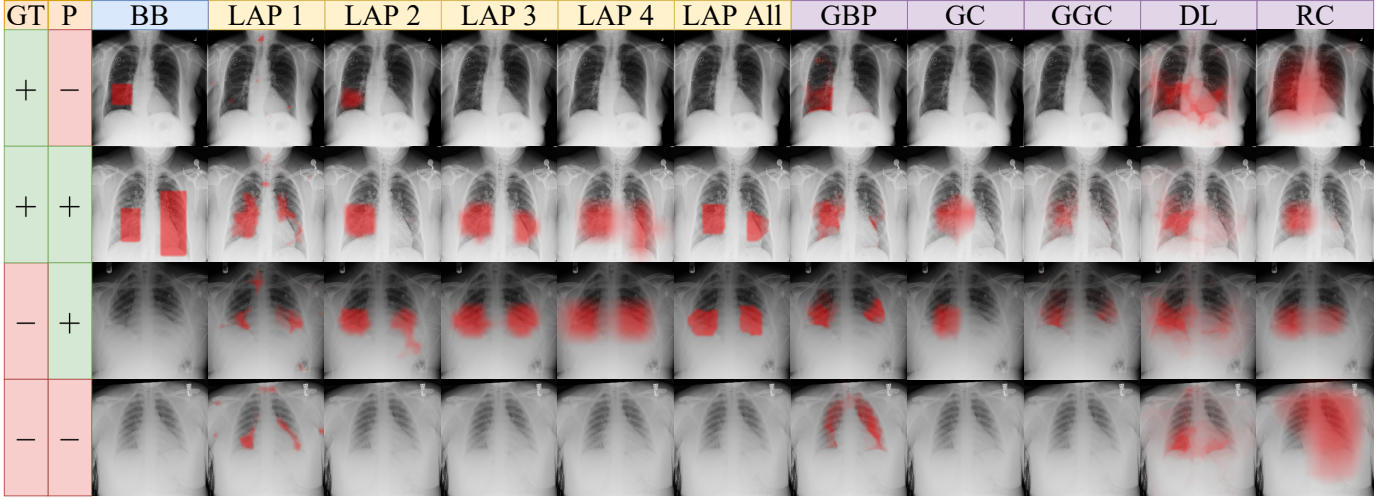


Fig. 2: Examples of BB-LAP Inception V3 interpretations (LAPs) compared to RSNA bounding boxes (BB) and other interpretation methods (GBP, GC, GGC, DL, and RC) on RSNA. LAP is faithful to the model’s prediction (P), and it shows from which layer the model has differed from the ground truth (GT).

a  $1 \times 1$  convolution layer with 1000 heads, each obligated to be partly active in its respective class samples and completely inactive otherwise. We used a  $1 \times 1$  convolution layer as the aggregation module to generate the final attention scores. We used our proposed weakly supervised loss beside the main cross-entropy loss. The details of the training configurations and hyper-parameters are described in the supplementary. We first trained only the LAP module while other parameters were frozen for two epochs. Then, we fine-tuned the fourth layer (containing the LAP) and the fully connected layer of the ResNet 50 for three epochs. The performances of the original model, the version with its LAP trained, and the final tuned one are presented in Tab. I. It is observable that LAP has adapted itself to the model while the performance is slightly improved.

In contrast to RSNA and CelebA, which had few simple concepts, ImageNet has 1000 concepts with objects of high-variance sizes. Therefore it is not straightforward to evaluate the LAP’s predictivity and faithfulness. We defined the concept size features,  $F_C \in \mathbb{R}^{1000}$ , as the sum of pixels’ importances in each concept map. Then we trained a 2-layer MLP network to classify the samples according to  $F_C$ . To evaluate the predictivity and faithfulness of the LAP, we compared the predictions of the mentioned MLP network with ground-truth and LAP-ResNet 50 (FT) predictions, respectively. The results are presented in Tab. I. Despite the complexity of the prediction task, the high similarity between many of the classes, and highly summarized information extracted from the concept maps, the LAP has achieved high predictivity and faithfulness.

We also compared the faithfulness of different interpretation methods on the tuned LAP ResNet 50 network on the ImageNet dataset by modifying the input images based on the interpretation scores. Faithfulness was evaluated by keeping  $k\%$  of pixels with the highest scores provided by the interpretation method and zeroing out the rest parts of the image, then passing the modified image as input through the network for re-evaluation. The results are presented in Fig. 4 for percentages of 10%, 30%, 50%, 70% and 90%. In this experiment, the interpretation scores were calculated based on the predicted class, and the results were also evaluated with respect to the original predictions. A faithful interpretation method would capture the effective regions for decision-making in the model, resulting in keeping the former decision for the modified image. Our method represents the highest faithfulness than other interpretation methods in Top1 and Top5 accuracies, introducing itself as the most confident one. We also repeated this experiment based on the ground truth labels to calculate the drop-in accuracies (supplementary material). Our method reached the highest accuracy for all percentages of pixels.

## V. CONCLUSION

This paper introduced Local Attention Pool (LAP), a concept-wise attention-based pooling method pluggable into any convolutional architecture, even an already trained one. We showed LAPs accommodate models with self-interpretability

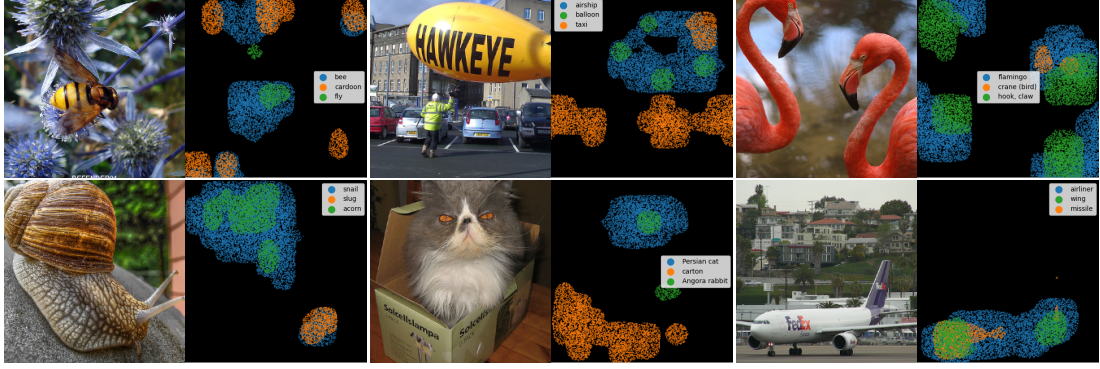


Fig. 3: Examples of LAP ResNet 50 interpretation on ImageNet. Different colors illustrate different concept heads. The legend shows the top-3 classes in order based on the model’s predictions (More examples are provided in the supplementary).

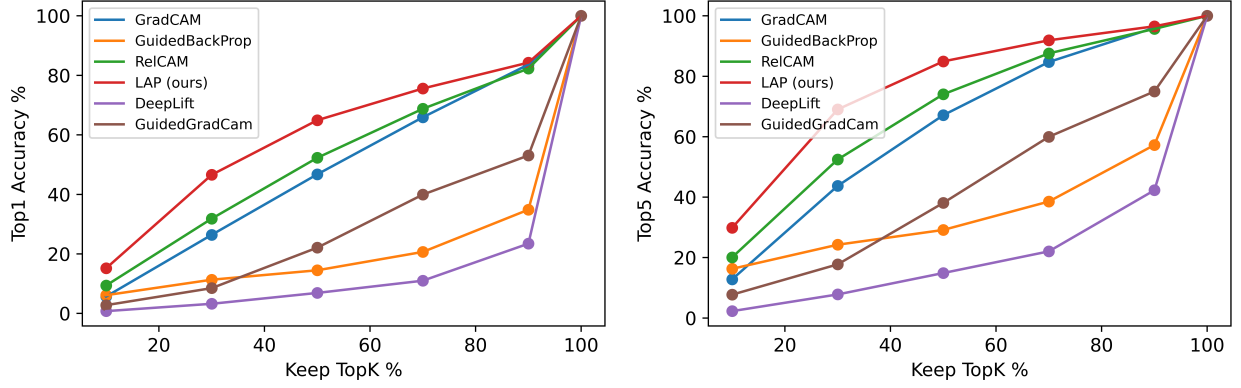


Fig. 4: Assessing the faithfulness of different interpretation methods, on the ImageNet dataset. Faithfulness is evaluated by keeping a ratio of pixels with the highest scores provided by the interpretation method (K%), then zeroing out the rest parts of the image, and evaluating the prediction based on the modified image with respect to the prediction of the original image. Our method both in Top1 and Top5 accuracies exceeds the other methods.

without performance loss. Furthermore, LAP attention maps proved their ability in explaining the model’s behavior faithful to its predictions compared to other explainers. They also can be used as standalone predictors. Their architecture can adapt to different domains and discriminate their concepts by weak or full supervision and knowledge sharing. In the future, we plan to use LAPs on tasks other than classification and improve the explainability by addressing the issues with receptive-field dependency.

## REFERENCES

- [1] Pneumonia detection challenge database (2018). Accessed April 10, 2021. [5](#)
- [2] Samira Abnar and Willem Zuidema. Quantifying attention flow in transformers. *Association for Computational Linguistics*, 2020. [2](#)
- [3] Dzmitry Bahdanau, Kyunghyun Cho, and Yoshua Bengio. Neural machine translation by jointly learning to align and translate. *arXiv preprint arXiv:1409.0473*, 2014. [1](#)
- [4] Alexander Binder, Grégoire Montavon, Sebastian Lapuschkin, Klaus-Robert Müller, and Wojciech Samek. Layer-wise relevance propagation for neural networks with local renormalization layers. In *International Conference on Artificial Neural Networks*, pages 63–71. Springer, 2016. [2](#)
- [5] Rich Caruana, Yin Lou, Johannes Gehrke, Paul Koch, Marc Sturm, and Noemie Elhadad. Intelligible models for healthcare: Predicting pneumonia risk and hospital 30-day readmission. In *Proceedings of the 21th ACM SIGKDD international conference on knowledge discovery and data mining*, pages 1721–1730, 2015. [1](#)
- [6] Hila Chefer, Shir Gur, and Lior Wolf. Generic attention-model explainability for interpreting bi-modal and encoder-decoder transformers. In *Proceedings of the IEEE/CVF International Conference on Computer Vision (ICCV)*, pages 397–406, October 2021. [2](#)
- [7] Hila Chefer, Shir Gur, and Lior Wolf. Transformer interpretability beyond attention visualization. In *Proceedings of the IEEE/CVF Conference on Computer Vision and Pattern Recognition (CVPR)*, pages 782–791, June 2021. [2](#)
- [8] Xi Chen, Yan Duan, Rein Houthooft, John Schulman, Ilya Sutskever, and Pieter Abbeel. Infogan: Interpretable representation learning by information maximizing generative adversarial nets. In *Proceedings of the 30th International Conference on Neural Information Processing Systems*, pages 2180–2188, 2016. [1](#)
- [9] Mengnan Du, Ninghao Liu, and Xia Hu. Techniques for interpretable machine learning. *Communications of the ACM*, 63(1):68–77, 2019. [1](#)
- [10] Alex A Freitas. Comprehensible classification models: a position paper. *ACM SIGKDD explorations newsletter*, 15(1):1–10, 2014. [1](#)
- [11] Ziteng Gao, Limin Wang, and Gangshan Wu. Lip: Local importance-based pooling. In *Proceedings of the IEEE/CVF International Conference on Computer Vision*, pages 3355–3364, 2019. [2](#)
- [12] Leilani H Gilpin, David Bau, Ben Z Yuan, Ayesha Bajwa, Michael Specter, and Lalana Kagal. Explaining explanations: An overview of interpretability of machine learning. In *2018 IEEE 5th International Conference on data science and advanced analytics (DSAA)*, pages 80–89. IEEE, 2018. [1](#)

[13] Bryce Goodman and Seth Flaxman. European union regulations on algorithmic decision-making and a “right to explanation”. *AI magazine*, 38(3):50–57, 2017. <sup>1</sup>

[14] Ran Gu, Guotai Wang, Tao Song, Rui Huang, Michael Aertsen, Jan Deprest, Sébastien Ourselin, Tom Vercauteren, and Shaoting Zhang. Ca-net: Comprehensive attention convolutional neural networks for explainable medical image segmentation. *IEEE Transactions on Medical Imaging*, 2020. <sup>2</sup>

[15] Kaiming He, Xiangyu Zhang, Shaoqing Ren, and Jian Sun. Deep residual learning for image recognition. In *Proceedings of the IEEE conference on computer vision and pattern recognition*, pages 770–778, 2016. <sup>5</sup>

[16] Been Kim, Martin Wattenberg, Justin Gilmer, Carrie Cai, James Wexler, Fernanda Viegas, et al. Interpretability beyond feature attribution: Quantitative testing with concept activation vectors (tcav). In *International conference on machine learning*, pages 2668–2677. PMLR, 2018. <sup>1</sup>

[17] Diederik P Kingma and Max Welling. Auto-encoding variational bayes. *arXiv preprint arXiv:1312.6114*, 2013. <sup>1</sup>

[18] Narine Kokhlikyan, Vivek Miglani, Miguel Martin, Edward Wang, Bilal Alsallakh, Jonathan Reynolds, Alexander Melnikov, Natalia Kliushkina, Carlos Araya, Siqi Yan, and Orion Reblitz-Richardson. Captum: A unified and generic model interpretability library for pytorch, 2020. <sup>5</sup>

[19] Alexander Kolesnikov, Alexey Dosovitskiy, Dirk Weissenborn, Georg Heigold, Jakob Uszkoreit, Lucas Beyer, Matthias Minderer, Mostafa Dehghani, Neil Houlsby, Sylvain Gelly, Thomas Unterthiner, and Xiaohua Zhai. An image is worth 16x16 words: Transformers for image recognition at scale. 2021. <sup>2</sup>

[20] Jeong Ryong Lee, Sewon Kim, Inyong Park, Taejoon Eo, and Dosik Hwang. Relevance-cam: Your model already knows where to look. In *Proceedings of the IEEE/CVF Conference on Computer Vision and Pattern Recognition*, pages 14944–14953, 2021. <sup>2</sup>

[21] Ziwei Liu, Ping Luo, Xiaogang Wang, and Xiaoou Tang. Deep learning face attributes in the wild. In *Proceedings of International Conference on Computer Vision (ICCV)*, December 2015. <sup>5</sup>

[22] Jiasen Lu, Jianwei Yang, Dhruv Batra, and Devi Parikh. Hierarchical question-image co-attention for visual question answering. *Advances in neural information processing systems*, 29:289–297, 2016. <sup>1</sup>

[23] Sébastien Marcel and Yann Rodriguez. Torchvision the machine-vision package of torch. In *Proceedings of the 18th ACM international conference on Multimedia*, pages 1485–1488, 2010. <sup>6</sup>

[24] Arnab Kumar Mondal, Arnab Bhattacharjee, Parag Singla, and Prathosh AP. xViTCOS: Explainable vision transformer based COVID-19 screening using radiography. July 2021. <sup>2</sup>

[25] Chris Olah, Alexander Mordvintsev, and Ludwig Schubert. Feature visualization. *Distill*, 2017. <https://distill.pub/2017/feature-visualization>. <sup>4</sup>

[26] Adam Paszke, Sam Gross, Francisco Massa, Adam Lerer, James Bradbury, Gregory Chanan, Trevor Killeen, Zeming Lin, Natalia Gimelshein, Luca Antiga, Alban Desmaison, Andreas Kopf, Edward Yang, Zachary DeVito, Martin Raison, Alykhan Tejani, Sasank Chilamkurthy, Benoit Steiner, Lu Fang, Junjie Bai, and Soumith Chintala. Pytorch: An imperative style, high-performance deep learning library. In H. Wallach, H. Larochelle, A. Beygelzimer, F. d’Alché-Buc, E. Fox, and R. Garnett, editors, *Advances in Neural Information Processing Systems 32*, pages 8024–8035. Curran Associates, Inc., 2019. <sup>5</sup>

[27] Mensah Kwabena Patrick, Adebayo Felix Adekoya, Ayidzoe Abra Mighty, and Baagyire Y Edward. Capsule networks—a survey. *Journal of King Saud University-computer and information sciences*, 2019. <sup>2</sup>

[28] F. Pedregosa, G. Varoquaux, A. Gramfort, V. Michel, B. Thirion, O. Grisel, M. Blondel, P. Prettenhofer, R. Weiss, V. Dubourg, J. Vanderplas, A. Passos, D. Cournapeau, M. Brucher, M. Perrot, and E. Duchesnay. Scikit-learn: Machine learning in Python. *Journal of Machine Learning Research*, 12:2825–2830, 2011. <sup>10</sup>

[29] Marco Tulio Ribeiro, Sameer Singh, and Carlos Guestrin. “ why should i trust you?” explaining the predictions of any classifier. In *Proceedings of the 22nd ACM SIGKDD international conference on knowledge discovery and data mining*, pages 1135–1144, 2016. <sup>2</sup>

[30] Olga Russakovsky, Jia Deng, Hao Su, Jonathan Krause, Sanjeev Satheesh, Sean Ma, Zhiheng Huang, Andrej Karpathy, Aditya Khosla, Michael Bernstein, Alexander C. Berg, and Li Fei-Fei. ImageNet Large Scale Visual Recognition Challenge. *International Journal of Computer Vision (IJCV)*, 115(3):211–252, 2015. <sup>6</sup>

[31] Sara Sabour, Nicholas Frosst, and Geoffrey E Hinton. Dynamic routing between capsules. *arXiv preprint arXiv:1710.09829*, 2017. <sup>1</sup>

[32] Ramprasaath R Selvaraju, Michael Cogswell, Abhishek Das, Ramakrishna Vedantam, Devi Parikh, and Dhruv Batra. Grad-cam: Visual explanations from deep networks via gradient-based localization. In *Proceedings of the IEEE international conference on computer vision*, pages 618–626, 2017. <sup>2</sup>

[33] Avanti Shrikumar, Peyton Greenside, and Anshul Kundaje. Learning important features through propagating activation differences. In *International Conference on Machine Learning*, pages 3145–3153. PMLR, 2017. <sup>2</sup>

[34] Karen Simonyan, Andrea Vedaldi, and Andrew Zisserman. Deep inside convolutional networks: Visualising image classification models and saliency maps. *arXiv preprint arXiv:1312.6034*, 2013. <sup>2</sup>

[35] Leon Sixt, Maximilian Granz, and Tim Landgraf. When explanations lie: Why many modified bp attributions fail. In *International Conference on Machine Learning*, pages 9046–9057. PMLR, 2020. <sup>1</sup>

[36] Jost Tobias Springenberg, Alexey Dosovitskiy, Thomas Brox, and Martin Riedmiller. Striving for simplicity: The all convolutional net. *arXiv preprint arXiv:1412.6806*, 2014. <sup>2</sup>

[37] Christian Szegedy, Vincent Vanhoucke, Sergey Ioffe, Jon Shlens, and Zbigniew Wojna. Rethinking the inception architecture for computer vision. In *Proceedings of the IEEE conference on computer vision and pattern recognition*, pages 2818–2826, 2016. <sup>5</sup>

[38] Gilles Vandewiele, Olivier Janssens, Femke Ongenae, Filip De Turck, and Sofie Van Hoecke. Genesim: genetic extraction of a single, interpretable model. In *NIPS2016, the 30th Conference on Neural Information Processing Systems*, pages 1–6, 2016. <sup>2</sup>

[39] Haofan Wang, Zifan Wang, Mengnan Du, Fan Yang, Zijian Zhang, Sirui Ding, Piotr Mardziel, and Xia Hu. Score-cam: Score-weighted visual explanations for convolutional neural networks. In *Proceedings of the IEEE/CVF conference on computer vision and pattern recognition workshops*, pages 24–25, 2020. <sup>2</sup>

[40] Tianfu Wu, Wei Sun, Xilai Li, Xi Song, and Bo Li. Towards interpretable r-cnn by unfolding latent structures. *arXiv preprint arXiv:1711.05226*, 2017. <sup>1</sup>

[41] Sen Yang, Zhibin Quan, Mu Nie, and Wankou Yang. Transpose: Keypoint localization via transformer. In *IEEE/CVF International Conference on Computer Vision (ICCV)*, 2021. <sup>2</sup>

[42] Quanzeng You, Hailin Jin, Zhaowen Wang, Chen Fang, and Jiebo Luo. Image captioning with semantic attention. In *Proceedings of the IEEE conference on computer vision and pattern recognition*, pages 4651–4659, 2016. <sup>1</sup>

[43] Quanshi Zhang, Ying Nian Wu, and Song-Chun Zhu. Interpretable convolutional neural networks. In *Proceedings of the IEEE Conference on Computer Vision and Pattern Recognition*, pages 8827–8836, 2018. <sup>1</sup>

[44] Xin Zhang, Liangxiu Han, Wenyong Zhu, Liang Sun, and Daoqiang Zhang. An explainable 3d residual self-attention deep neural network for joint atrophy localization and alzheimer’s disease diagnosis using structural MRI. *IEEE Journal of Biomedical and Health Informatics*, pages 1–1, 2021. <sup>2</sup>

[45] Bolei Zhou, Aditya Khosla, Agata Lapedriza, Aude Oliva, and Antonio Torralba. Learning deep features for discriminative localization. In *Proceedings of the IEEE conference on computer vision and pattern recognition*, pages 2921–2929, 2016. <sup>2</sup>

## APPENDIX

The loss function for full supervision is similar to the weakly supervised concept discrimination loss of Sec. 3.3. We used experts' annotated bounding boxes as the ground truth for active pixels for the first term. Because all the areas under a bounding box may not belong to infection zones, we applied the loss on half of the pixels with higher importance probability within the box only. All the zones out of the bounding boxes correspond to non-infection areas. We applied the second term to all of them. The third term was used similarly as the weakly supervised loss.

### A. RSNA

For weak supervision, we used cross-entropy loss on the classification head, concept-discrimination loss, and inter-LAPs concordance loss with weights of 1, 0.25 per LAP, and 0.25 per LAP pair, respectively. The hyper-parameters of the concept-discrimination loss were as follows: MinAR = 0.1, MaxAR = 0.5, IAR = 0.1. The first two were set based on the possible range of concept sizes, i.e., infection, in the positive samples. We chose the median and maximum of the infection bounding-boxes areas as the mentioned bounds. The third was set to 0.1 to avoid fading its corresponding loss term. For full supervision, we used cross-entropy loss on the classification head alongside cross-entropy loss on LAPs considering experts' bounding boxes as the ground truth with weights of 1 and 0.25 per LAP, respectively.

We trained the models for 300 epochs, where we observed convergence due to no change in the last 50 epochs. We selected the model related to the epoch with the best performance on validation data as the final model. We used batches of size 64 (32 healthy and 32 pneumonia samples) and the ADAM optimizer with an initial learning rate of  $10^{-4}$  and a decay coefficient of  $10^{-6}$  in training. The models were trained on a GEFORCE RTX 2080 Ti GPU.

### B. CelebA

We trained LAP-extended models with our proposed weak knowledge injection method. We used the same loss terms and procedure of choosing the hyper-parameters of the concept-discrimination loss as Appendix A. The hyper-parameters were set as follows: MinAR = 0.02, MaxAR = 0.2, IAR = 0.01 for the first two heads and MaxAR = 0.1, without MinAR and IAR for the common concept head. Choosing these hyper-parameters was the same as Appendix A for the CelebA dataset. We trained the networks for 12 epochs, where we observed convergence. The other training hyper-parameters were also the same as in Appendix A.

### C. ImageNet

We used our proposed weakly supervised loss (MinAR and IAR of 0.01, without MaxAR) with a factor of 0.125 beside the main cross-entropy loss. We first trained only the LAP module while other parameters were frozen for two epochs using the ADAM optimizer with an initial learning rate of  $10^{-4}$  and a decay coefficient of  $10^{-6}$ . Then, we fine-tuned the fourth layer (containing the LAP) and the fully connected layer of the ResNet 50 for three epochs using a stochastic gradient descent optimizer with an initial learning rate of  $10^{-3}$  and a decay coefficient of  $10^{-6}$ .

We first normalized each importance map by its maximum value according to their papers to find a global threshold for other explainer methods. Then we created a dataset from the normalized pixel-wise interpretation scores over the validation samples. We assigned the positive label to all the pixels under the experts' annotated boxes and the negative to the others. We used RidgeClassifier of sklearn [28] for the classification of the pixels. Due to a large number of pixels, we used the *lsqr* solver with a tolerance of  $10^{-3}$ , alpha of 0.01, and set the maximum iterations to 100. We also used balanced weighting to address the issue with the highly imbalanced dataset. We used the point with the prediction label equal to zero as the threshold for binarization. We applied this method for each trained model separately and used the resulting threshold to evaluate the model's interpretations.

LAPs can be considered a sequence of information through the depth of the network. Shallower LAPs cannot capture enough information due to their low receptive field. Therefore, they are likely to make more mistakes. Some pixels may have been assumed to be important but were found unimportant in the deeper layers and vice versa. But because of the low receptive field and high resolution, they produce more detailed maps. We devised an algorithm to integrate interpretations from the final LAP layers iteratively to the initial layers. In this way, we can have both accuracy and resolution. The procedure's pseudo-code is presented in Algorithm 1, in which  $\alpha$  is the decay factor to adjust the impact of shallower LAPs. Iteratively, the algorithm modifies the current integrated map,  $R_{l+1}$ , with the current LAP attention map,  $P_l$ . Considering one pixel of  $R_{l+1}$ ,  $r_{l+1} \in \mathbb{R}$ , and the set of its corresponding pixels in  $P_l$ ,  $p_l \in \mathbb{R}^{H_K \times W_K}$ , if  $r_{l+1}$  is active, i.e., greater than 0.5, at least one pixel in the corresponding zone must have been responsible. If any pixel of the  $p_l$  is active, the credit only belongs to the active pixels. Otherwise, the current LAP has not comprehended the importance of this zone. Therefore the credit belongs to all of them. Using this scheme, we prune the produced importance map from the last LAP, expected to be the most accurate, to the first. In the case of choosing the topK pixels based on the size of the ground truth bounding box, the scores have been added without being clipped to keep the order of scores below 0.5 and have a proper selection.

**Algorithm 1** Pseudo-code for integrating the currently integrated map pixel on the position  $(i, j)$  from the  $L^{\text{th}}$  LAP to  $l + 1^{\text{th}}$  LAP with  $l^{\text{th}}$  LAP attention map in the corresponding kernel. This procedure is repeated for each pixel of each LAP layer, from  $L$  to 1.

```

1:  $\alpha \leftarrow 0.8$  ▷ the impact decay factor
2:  $L \leftarrow$  The number of LAP layers
3: procedure INTEGRATEPIXEL( $R, P, l, i, j, H_K, W_K$ )
4:    $p_l \leftarrow \text{GETKERNEL}(P_l, i, j, H_K, W_K)$  ▷  $l^{\text{th}}$  LAP attention map for  $(i, j)$ 's corresponding kernel of size  $H_K \times W_K$ 
5:   if  $l = L$  then
6:     return  $p_l$ 
7:   end if
8:    $r_{l+1} \leftarrow R_{l+1}[i, j]$  ▷ current integrated map pixel from  $L^{\text{th}}$  LAP to  $l + 1^{\text{th}}$  LAP
9:    $r_l \leftarrow r_{l+1}$  repeated to size  $H_K \times W_K$  ▷ The result integrated map
10:  if  $r_{l+1} \geq 0.5$  &  $\max\{p_l\} \geq 0.5$  then
11:    for  $i' : [0, H_K)$  do
12:      for  $j' : [0, W_K)$  do
13:         $p \leftarrow p_l[i', j'] \times \alpha^{L-l}$  ▷ Apply the decay factor
14:        if  $p_l[i', j'] \geq 0.5$  then
15:           $r_l[i', j'] \leftarrow \max\{r_{l+1}, p\}$ 
16:        else
17:           $r_l[i', j'] \leftarrow p$ 
18:        end if
19:      end for
20:    end for
21:  end if
22:  return  $r_l$ 
23: end procedure

```

We compared the faithfulness of different interpretation methods on the tuned LAP ResNet 50 network on the ImageNet dataset by modifying the input images based on the interpretation scores. Faithfulness was evaluated by keeping  $k\%$  of pixels with the highest scores provided by the interpretation method and zeroing out the rest parts of the image, then passing the modified image as input through the network for re-evaluation. The results are presented in Fig. 5 for percentages of 10%, 30%, 50%, 70% and 90%. In this experiment, the interpretation scores were calculated based on the ground truth class, and the results were also evaluated with respect to the ground truth. A faithful interpretation method would capture the effective regions for decision-making in the model, keeping the former decision for the modified image. Our method represents the highest faithfulness than other interpretation methods in Top1 and Top5 accuracies, introducing itself as the most confident.

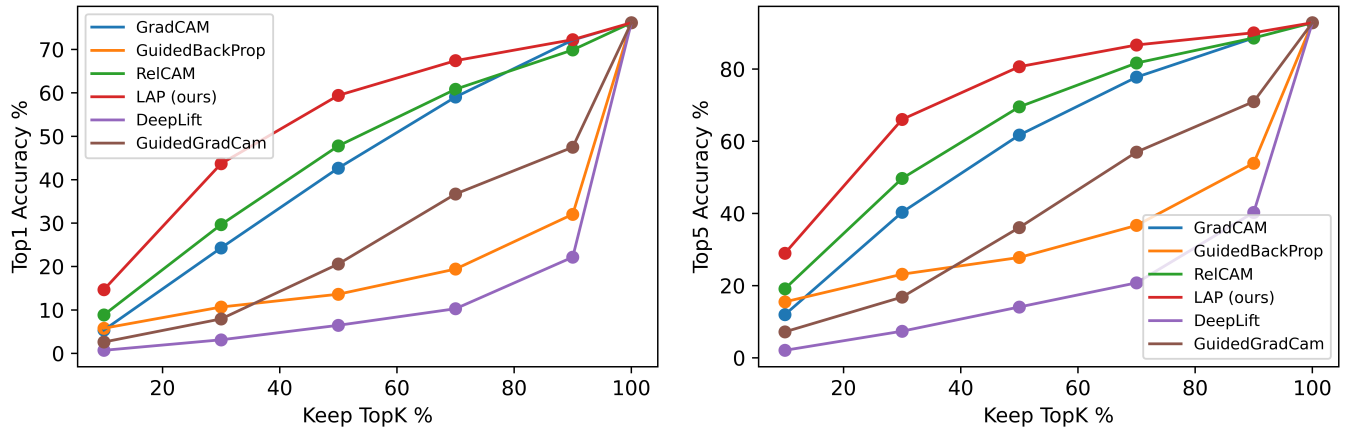


Fig. 5: Assessing the faithfulness of different interpretation methods on the ImageNet dataset. Faithfulness is evaluated by keeping a ratio of pixels with the highest scores provided by the interpretation method ( $K\%$ ) for the ground truth class, then zeroing out the rest parts of the image, and evaluating the prediction based on the modified image with respect to the prediction of the original image. Our method in Top1 and Top5 accuracies exceeds the other methods.

We conducted an ablation study on the RSNA dataset using the ResNet 18 network to assess the effect of different loss

terms and hyperparameters. The results are presented in Tab. III. In 2 settings, the network was trained without applying the concordance loss and without using any loss term to the LAP layers. The binarized interpretation maps were evaluated based on IoU with the ground truth bounding boxes. It is observed both losses have enhanced interpretations. In the case of applying no loss term to the LAPs, even though the network has been free, it has tended to pay attention to the infected regions. In 8 other settings, the network was trained with different values for MinAR, MaxAR, and IAR. The values of the hyperparameters are presented in Tab. IV. It is observed that the selected setting, based on the domain's properties according to Appendix A, has achieved the second-highest IoU with a slight difference from the first rank. Notably, the setting achieving the first rank had the same MinAR and MaxAR, which were selected based on the domain. The only difference was lower IAR which had put a higher weight on the mistakes of the negative cases. In all of the proposed settings, using a value much lower and much higher than the selected MinAR has affected the results the most. The reason is that the chosen value, the expected size of the distinguishing part, explores the right amount of the image. A much higher value will force the network to find irrelevant pixels as distinguishing parts, which will deteriorate the gradient flow. A much lower value will prevent the network from exploring all the distinguishing parts, and it would only learn highly distinguished pixels and lose its generalization. A low value for MaxAR will also force the network to keep the distinguishing region small and will cause problems in cases with large infected zones. This experiment shows that hyper-parameters can be selected according to the method described in Appendix A, and there is no need to try many different values. Noteworthy, all configurations but the ones related to high MinAR and all-low configuration are highly above interpretations made by other methods on the network trained by the selected values.

TABLE III: IoUs of infection bounding boxes of RSNA and binarized interpretation maps of the LAP ResNet 18 network trained with different configurations using two binarization approaches, thresholding (TH) and topK selection by ground truth (TK). Configurations have three locations for MinAR, MaxAR, and IAR, respectively. — has been used for the unchanged value,  $L$  for a lower value, and  $H$  for a higher value with respect to the selected config. *No C* and *No L* stand for not applying concordance loss and the whole proposed loss in LAPs, respectively. Notably, applying both loss terms has enhanced the interpretations. Additionally, the selected config based on the domain knowledge has achieved the second-highest value with a slight difference from the 1st rank, which validates the selection methodology.

Method	—	No C	No L	L—	-L-	-L	LLL	H—	-H-	-H	HHH
TH	36.26	30.17	26.32	30.27	36.03	37.79	28.64	25.10	35.12	33.31	22.03
TK	44.29	43.60	32.78	36.74	39.83	45.87	40.48	42.05	41.21	38.01	36.57

TABLE IV: The values used for MinAR, MaxAR, and IAR hyperparameters in the ablation study of RSNA.

Type	-	L	H
MinAR	0.1	0.01	0.5
MaxAR	0.5	0.1	0.9
IAR	0.1	0.01	0.5

Due to the limited number of pages in the main paper, we have provided more images interpreted with LAP for RSNA, CelebA, and Imagenet in Figs. 6, 7 and 8, respectively.

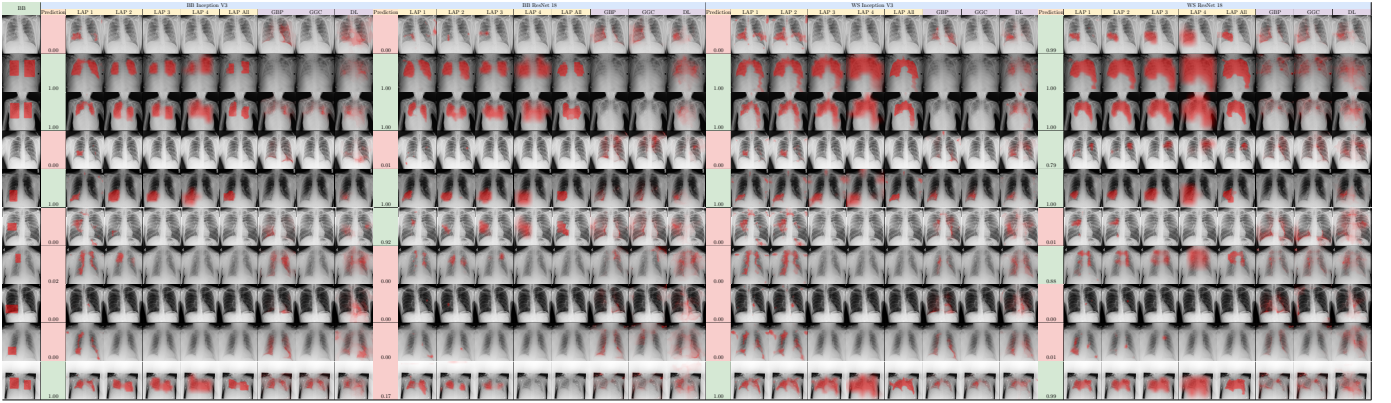


Fig. 6: Examples of all models' interpretations (LAPs) compared to RSNA bounding boxes (BB) and other interpretation methods (GBP, GC, GGC, DL, and RC) on the RSNA dataset. The probability assigned by each model is presented, and the background color represents the final decision of the model. Despite other methods, LAP interpretation is faithful to the model's prediction, and they help diagnose the layer from which the model has made a mistake in decision-making.

- **RSNA:** The dataset is freely available for download from [Kaggle](#). Based on the competition website "the competition data is allowed to be used for the competition, participation on Kaggle website forums, academic research and education, and

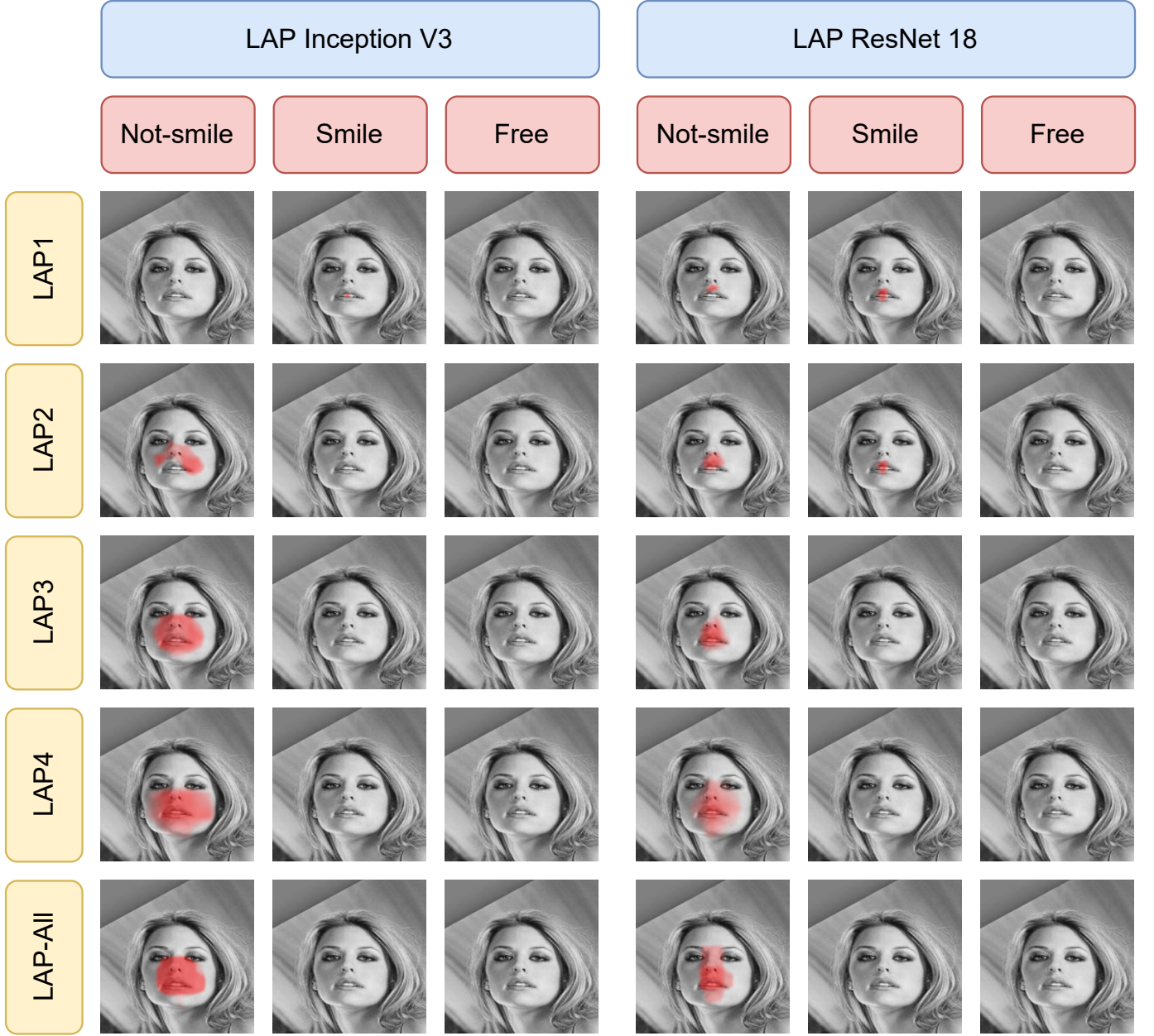


Fig. 7: Examples of interpretations on the CelebA dataset for a non-smiling image. The Not-smile, Smile, and free columns show the active pixels in the related channels. For both LAP Inception and LAP ResNet networks, teeth have been a sign of smiling in the initial layers, but the decision has been corrected in the next layers. The model has not highlighted anything in the free head, which states the two first heads had been enough.

other commercial or non-commercial purposes as long as the attribution for the dataset and the individual items (sound files) are provided when required.”

- **CelebA:** The dataset is freely available for download from [CelebA website](#). Based on [the website](#), ”The CelebA dataset is available for non-commercial research purposes only”.
- **ImageNet:** The dataset of ImageNet Large Scale Visual Recognition Challenge 2012-2017 is freely available for download from [the ImageNet website](#). Based on [the website](#), ”researchers shall use the Database only for non-commercial research and educational purposes”.

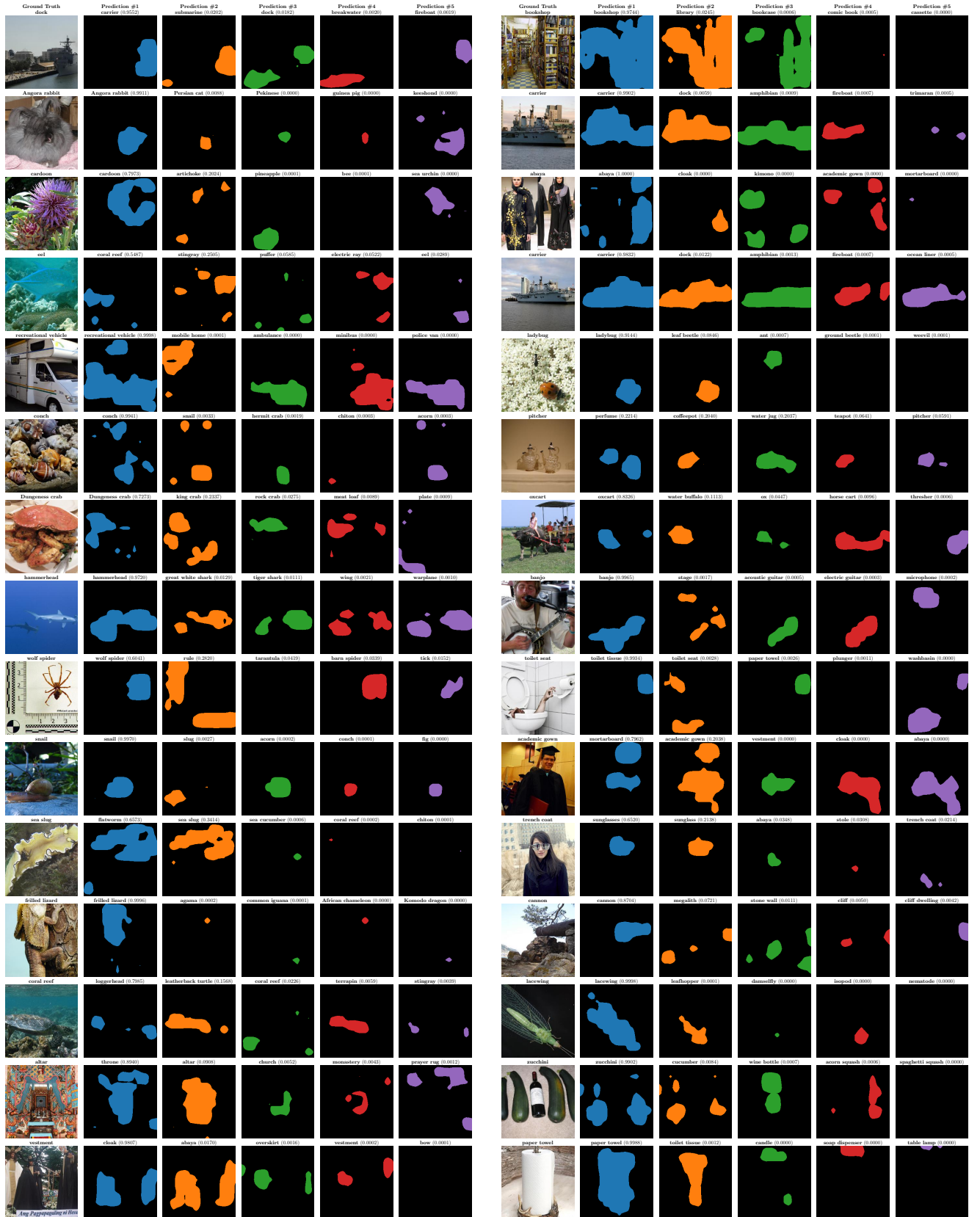


Fig. 8: Further Concept-wise interpretation Examples of LAP ResNet 50 on ImageNet dataset. For each example, concept heads related to the top-5 predictions of the model are illustrated separately. The probability assigned by the model for each concept head is presented too. The interpretation maps clarify why the model has chosen each class as one of its top 5.